IMAGE FORMATION METHODS IN QUANTITATIVE ACOUSTIC MICROSCOPY

Jonathan Mamou and Daniel Rohrbach

F. L. Lizzi Center for Biomedical Engineering
Riverside Research
New York, NY, USA

ABSTRACT

Quantitative acoustic microscopy (QAM) is an imaging modality which uses very-high-frequency ultrasound (i.e., >200 MHz) to form two-dimensional (2D) quantitative images of acoustical and mechanical properties of soft tissues with microscopic resolution (i.e., better than 8 μm). The key component of a QAM system is the ultrasound transducer which must be broadband, have a very small F-number (i.e., < 1.2), and good sensitivity. In this study, two QAM systems based on a 250-MHz and a 500-MHz transducer are presented, yielding 2D quantitative images at spatial resolution of 7 μm and 4 μm respectively. Thin tissue sections obtained using a microtome or cryotome are raster scanned with precise motors and pulse-echo RF signals are digitized. Inverse models are then used to process each RF signal individually to estimate acoustic impedance, speed of sound, and acoustic attenuation as well as derived parameters such as bulk modulus, mass density, and compressibility. To illustrate the QAM technology and signal processing algorithms, images from cancerous human lymph nodes and ophthalmologic samples are presented and coregistered with histology photomicrographs.

Index Terms— Ultrasound, acoustic microscopy, very-high frequency

1. INTRODUCTION

Acoustic microscopy is a well-established imaging modality which has been used for non-destructive testing as well as for assessing material properties of hard and soft tissues. Some seminal work dates back from the 70s [1, 2, 3]. Since then acoustic microscopy has been applied successfully to characterizing various soft tissues such as coronary-artery, skin, liver, and muscle tissue [4, 5, 6]. Recently, the term quantitative acoustic microscopy (QAM) has been introduced to emphasize the quantitative nature of the more modern implementations of acoustic microscopy. In particular, when measurements are performed using a through transmission approach.

In this study, two innovative QAM systems are presented. While both share some hardware (e.g., motor stages, digitizer oscilloscope), they employ two distinct transmit-receive lines and use two different transducers operating at center frequencies of 250 and 500 MHz, respectively. The measurement forward model is presented and two different inverse models are used for image formation and briefly discussed. Finally, illustrative QAM images are presented from cancerous human lymph nodes and ophthalmologic samples.

Supported in part by NIH grant EB016117

2. METHODS

2.1. QAM systems and data acquisition

The QAM systems were designed at Riverside Research and Fig. 1 shows a picture of the 250-MHz QAM system. This system uses a 300-MHz monocyte pulser (GEOZON-DAS, Vilnius-09, Lithuania) to excite a 250-MHz transducer (Fraunhofer IBMT with F-number 1.16 and 160-MHz bandwidth). Received radio-frequency (RF) signals were amplified (MITEQ, Hauppauge, NY, USA) and digitized at 2.5 GHz using a 12-bit oscilloscope (Teledyne LeCroy, Chestnut Ridge, NY, USA). The 500-MHz system is nearly identical except that it uses a 500-MHz monocycle pulse to excite a 500-MHz transducer (Fraunhofer IBMT with F-number 1.08 and 264-MHz bandwidth). Therefore, both systems share the same operating block diagram which is shown in Fig. 2.

The specimens are raster scanned by mounting a microscopy slide in an upside-down configuration (see magnification in Fig. 1) using a three-axis, high-precision scanning stage. The distance between adjacent scan location were set at 2 μm and 1 μm for the 250-MHz and 500-MHz QAM system, respectively. The QAM systems were controlled by a dedicated computer using custom LabVIEW software.

2.2. Image formation

To form 2D images, each RF signal is processed individually to yield acoustic impedance (Z), speed of sound (c), and attenuation (A) in tissue. Then the values of Z and c are used to compute additional parameters such as bulk modulus (K), mass density (ρ), and compressibility (κ). A final 2D map of each acoustic property is then obtained by combining the estimates from all scanned locations together.

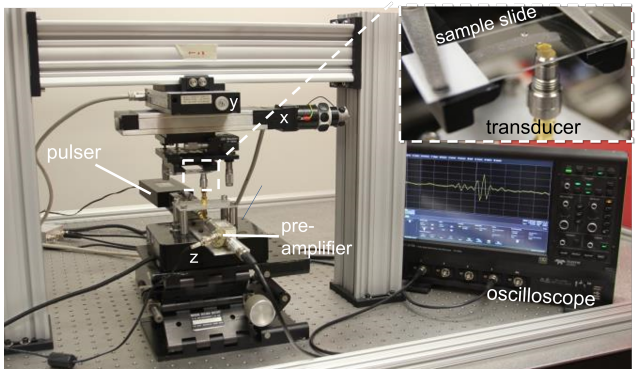

Fig. 1. Photograph of the 250-MHZ system, and magnification showing the transducer and the sample (upper right corner).

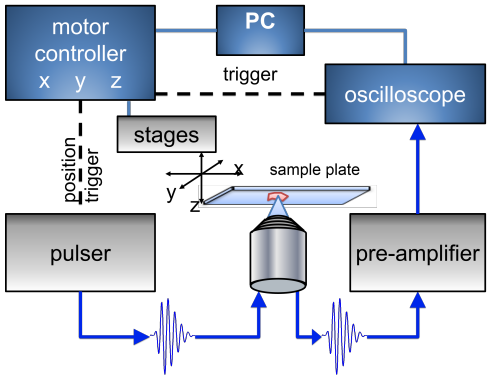

Fig. 2. Operating block diagram of the QAM systems.

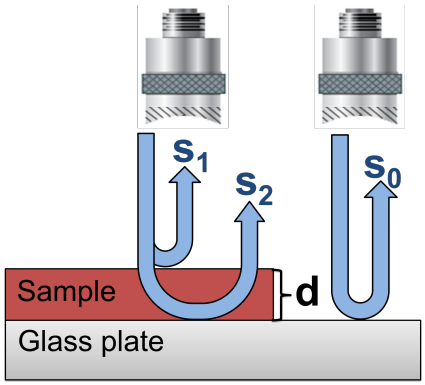

Fig. 3. Cartoon showing measurement principle at a tissue location (i.e., s_1 and s_2) and at a glass-slide only location (i.e., s_0)

The estimation method assumes that each received signal ($s(t)$) is composed of two reflected signals, one from the water-tissue interface (i.e., s_1) and one from the tissue-glass interface (i.e., s_2) as illustrated in Fig. 3:

$$\begin{aligned} s(t) &= s_1(t) + s_2(t) && (1)\\ &= C_1 s_0^*(t-t_1) + C_2 s_0^*(t-t_2), && (2)\end{aligned}$$

which means that the sample signals are the sum of two weighted and delayed version of the reference signal (s_0). The '*' symbol represents frequency-dependent attenuation effects. In practice, s_0 is obtained from a location devoid of tissue and is therefore composed of one reflection due to the water-glass interface as shown in Fig. 3.

By taking the Fourier transform of Eq. (2), we obtain:

$$\begin{aligned} S(f) = S_0(f)[&C_1 \exp(2\pi f(\beta_1 + j(t_1 - t_0)\\ &+C_2 \exp(2\pi f(\beta_2 + j(t_2 - t_0)], \end{aligned} \quad (3)$$

where β_1 and β_2 is the attenuation coefficient suffered by the first and second signal (in Np/Hz), respectively. Finally, Eq. (3) is used to obtain, $N(f)$, the normalized spectrum:

$$\begin{aligned} N(f) = \frac{S(f)}{S_0(f)} =&C_1 \exp(2\pi f\,[\beta_1 + j(t_1 - t_0)])\\ &+C_2 \exp(2\pi f\,[\beta_2 + j(t_2 - t_0)]) \end{aligned} \quad (4)$$

Two inverse models have been investigated to obtain acoustic parameter using the forward model described in Eq. (4). The first one has been described previously in [7] and the other method assuming Eq. (4) is an autoregressive (AR) model of a certain order (e.g., order 5) in the frequency domain. The AR model elegantly exploit that the normalized spectrum is the sum of two complex exponential series of the discretized frequency. Although both approaches have differences, they essentially lead to estimates of the quantities $C1$, C_2, $t_1 - t_0$, $t_2 - t_0$, and β_2. (The first reflection is assumed to not suffer any attenuation and therefore we assume that $\beta_1 = 0$.)

Then, the acoustic parameters are estimated by easily inverting the following equations which are obtained from first principles:

$$\begin{aligned} t_1 - t_0 &= \frac{2d}{c_w} && (5)\\ t_2 - t_0 &= \frac{2d}{c} - \frac{2d}{c_w} && (6)\\ C_1 &= \frac{Z - Z_w}{Z + Z_w}\frac{Z_g + Z_w}{Z_g - Z_w} && (7)\\ \beta_2 &= 2dA, && (8)\end{aligned}$$

where d is the unknown sample thickness, c, Z and A are the unknown sample acoustic speed of sound (in m/s), impedance (in MRayl), and attenuation (in Np/Hz/m), respectively (linear acoustic attenuation is an accepted assumption within a

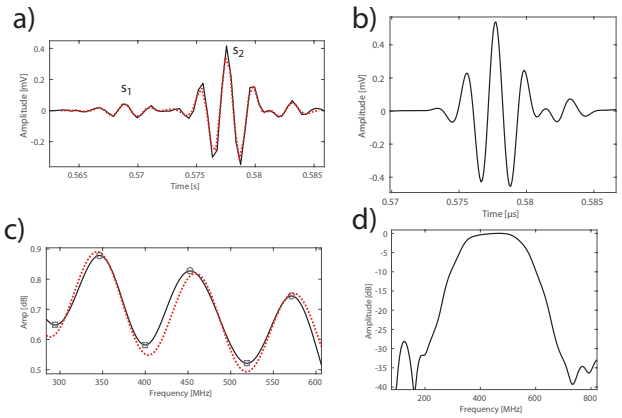

Fig. 4. Illustrative experimental signals acquired with the 500-MHz QAM system. a) Echo signal from tissue (i.e., $s(t) = s_1(t) + s_2(t)$), b) reference signal (i.e., $s_0(t)$), c) normalized spectrum (i.e., $N(f)$), and d) spectrum of b) (i.e., $10\log_{10}\left(|S_0(f)|^2\right)$).

given bandwidth [8]). (c_w and Z_w are the known speed of sound and acoustic impedance of water. Z_g is the known acoustic impedance of glass.)

3. RESULTS

3.1. Illustrative signals and resolution

Figure 4 shows illustrative experimental signals acquired from a human lymph node thin section using the 500-MHz QAM system. Figure 4a reveals that the experimental signal (in black) follows well the forward model of Eq. (1) because two well-separated signals (s_1 and s_2) are observed. Figures 4b and 4d show the reference signal and his spectrum; they demonstrate the broadband nature of the transducer and of the transmit-receive electronic. The normalized spectrum is shown in black in Fig. 4c and shows a pseudo-periodic signal with a slow decrease as frequency increases. The periodicity is exploited in the inverse models to find $t_1 - t_0$ and $t_2 - t_0$ and the slope of the decrease is related to β_2. Finally, for illustrative purposes the red-dotted lines in Figs. 4a and 4c also show the fit obtained using the inverse model described in [7] (i.e., Eqs. (2) and (4), respectively, with estimated parameters from Eqs. (5)-(8)).

In another set of experiments, images were formed from a USAF 1951 optic resolution target, and results confirmed that images formed using the 250-MHz and 500-MHz QAM systems had a spatial resolution better than 7 μm and 4 μm, respectively.

3.2. Cancerous human lymph nodes

In a previous project, QAM was investigated to assess mechanical properties of lymph nodes excised from cancer patients. The motivation for these studies was threefold. First, QAM provides previously-unavailable values of acoustic properties of tissue constituents at very fine resolution (including cancer cells). Second, 2D impedance maps (i.e., 2DZMs) are a useful tool to characterize ultrasound scattering [9] and could be used to improve sensitivity and specificity of quantitative ultrasound methods further in excised lymph nodes or even *in vivo*. And third, QAM can improve the understanding of cancer progression in lymph nodes by providing mechanical properties of tissues at a microscopic scale. Figure 5 shows results obtained from an illustrative lymph node acquired from a colorectal cancer patient. This lymph node was found to be metastatic and therefore, the 2DZM shows striking differences between cancerous and non-cancerous tissue which in turn could explain ultrasound scattering observed at lower frequencies.

3.3. Human eyes

In more recent studies, QAM was used to assess ophthalmic samples because many eye conditions are believed to affect the mechanical properties of the eye (e.g., myopia, keratoconus, glaucoma, etc.). Figure 6 shows data acquired from human eye using the 250-MHz QAM system. The image region is near the optic nerve which is an area greatly affected by glaucoma. Figure 6b displays a 2D map of the K because it can be related to mechanical properties of the eye which are most likely to be affected by disease.

4. CONCLUSIONS

Quantitative acoustic microscopy in soft tissue can provide unique information about a wide range of tissues as illustrated here. In addition, from a signal-processing standpoint, the forward model outlined in Eq. (1) is relatively simple and a good description of what is experimentally observed (as illustrated in Fig. 4a). In this study, two inverse models were successfully used to form images. Future studies will carefully evaluate the bias and variance of these inverse models and determine whether one is better for experimental data.

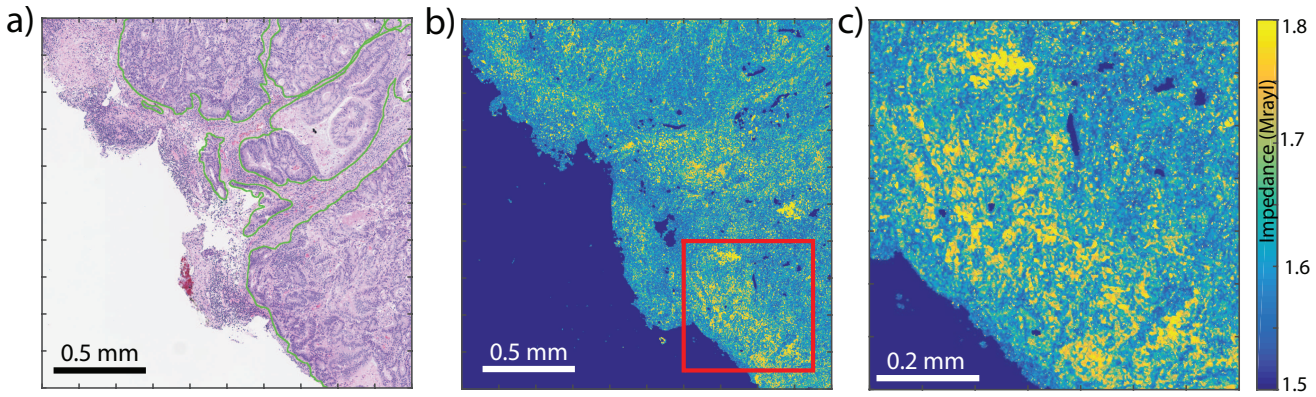

Fig. 5. Site-matched maps of (a) H&E-stained digital photomicrograph, (b) acoustic impedance, and (c) enlarged acoustic impedance obtained from the red rectangle in (b). All these images were obtained from a lymph node from a colon-cancer patient using the 500-MHz QAM system. In (a), metastases (i.e., adenorcarcinoma) were demarcated in green. The rest of the tissue is fibrosis mixed with some lymphocytes and macrophages. The parameter map was obtained using the inverse model described in [7]

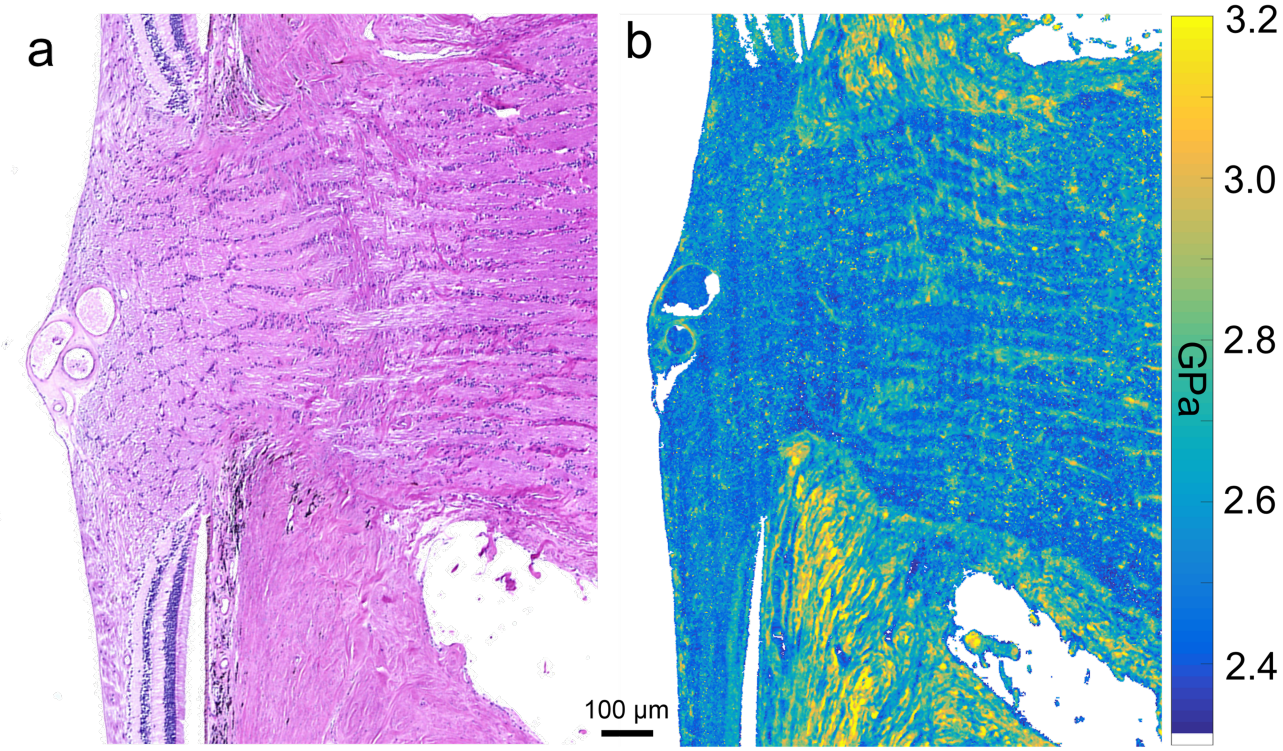

Fig. 6. Site-matched maps of (a) H&E-stained digital photomicrograph, (b) bulk-modulus image obtained from the optic nerve region of a human eye using the 250-MHz QAM system.The parameter map was obtained using the inverse model described in [7]

5. REFERENCES

[1] R. A. Lemons, "Acoustic microscopescanning version," *Applied Physics Letters*, vol. 24, no. 4, pp. 163, 1974.

[2] M F Marmor, H K Wickramasinghe, and R A Lemons, "Acoustic microscopy of the human retina and pigment epithelium," *Investigative ophthalmology & visual science*, vol. 16, no. 7, pp. 660–666, July 1977.

[3] C.F. Quate, A. Atalar, and H.K. Wickramasinghe, "Acoustic microscopy with mechanical scanning A review," *Proceedings of the IEEE*, vol. 67, no. 8, pp. 1092–1114, 1979.

[4] C. M. W. Daft and G. A. D. Briggs, "The elastic microstructure of various tissues," *The Journal of the Acoustical Society of America*, vol. 85, no. 1, pp. 416, 1989.

[5] N Hozumi, R Yamashita, C-K Lee, M Nagao, K Kobayashi, Y Saijo, M Tanaka, N Tanaka, and S Ohtsuki, "Time-frequency analysis for pulse driven ultrasonic microscopy for biological tissue characterization," *Ultrasonics*, vol. 42, no. 1-9, pp. 717–722, Apr. 2004.

[6] Y Saijo, M Tanaka, H Okawai, H Sasaki, S I Nitta, and F Dunn, "Ultrasonic tissue characterization of infarcted myocardium by scanning acoustic microscopy," *Ultrasound in medicine & biology*, vol. 23, no. 1, pp. 77–85, 1997.

[7] Daniel Rohrbach, Anette Jakob, Harriet Lloyd, Steffen Tretbar, Ronald H. Silverman, and Jonathan Mamou, "A Novel Quantitative 500-MHz Acoustic-microscopy System for Ophthalmologic Tissues," *IEEE Transactions on Biomedical Engineering*, in press, 2016.

[8] Francis A. Duck, "Chapter 4 - acoustic properties of tissue at ultrasonic frequencies," in *Physical Properties of Tissues*, Francis A. Duck, Ed., pp. 73 – 135. Academic Press, London, 1990.

[9] Jonathan Mamou, Michael L. Oelze, William D. O'Brien, and James F. Zachary, "Identifying ultrasonic scattering sites from three-dimensional impedance maps," *The Journal of the Acoustical Society of America*, vol. 117, no. 1, pp. 413–423, Jan. 2005.